Multiscale fracture and damage zone characterization in a tight sandstone reservoir, Sichuan Basin, China

Zonghu Liao[1], Weilun Chen[2], Xiaofeng Chen[3], Huayao Zou[1], and Fang Hao[4]

Abstract

Fractures within fault damage zones are crucial for the migration of subsurface fluids, which is challenging the characterization of the fractures and damage zones in the subsurface due to the lack of subsurface data. We have investigated the fractures and fault damage zones in the tight sandstone gas-bearing Xujiahe Formation in the northeast Sichuan Basin, China, based on a comprehensive study of seismic data, well log, core, as well as field observations. We have demonstrated the structure and distribution of damage zones from the basin-scale down to the microscale. The core samples find mostly opening-mode microfractures that can be subcritically generated under low tectonic stress fields since the Late Triassic-Middle Jurassic. These opening-mode microfractures in such ultra-low-permeability sandstone are likely to provide a storage volume for coal gas to accumulate. Macrofractures from image logging and outcrop display well-developed joint networks within the sandstone. The basin-wide distribution of such macrofractures implies potential conduits for gas migration during basin uplift in the Cretaceous. The damage zones are formed and controlled by a system of reverse faults, with thicknesses ranging 100–1500 m. The multiscale analysis of fractures implies that, for the tight sandstone within the Xujiahe Formation, the fractures and damage zones are likely to control the gas migration and accumulation during the tectonic transformation from the Late Cretaceous to the Quaternary Period. The overpressure history, coupled with the fracture system, enhances the redistribution of the gas reservoir. This approach and these data lead to a more in-depth understanding of the fractures and damage zones on a regional scale, which could extend to hydraulic and mechanical characterization of damage zones in the upper crust.

Introduction

Faults are commonly described as zones with a fault core and a surrounding damage zone, which differs structurally, mechanically, and petrophysically from the undeformed host rock (protolith) (Chester and Logan, 1986; Caine et al., 1996; Sagy et al., 2001; Katz et al., 2003; Savage and Brodsky, 2011). The damage zone is determined by the structures that formed as a result of the faulting process, which may present complex nature of its fracture networks, owing to fault-related diagenesis, segmentation, and evolution (Laubach et al., 2014). With limited data, it is challenging to evaluate the structure of damage zones in the subsurface that significantly affects the migration, accumulation, and leakage of subsurface fluids (Caine et al., 1996; Faulkner et al., 2010; Ellis et al., 2012; Busetti et al., 2012).

Fault damage zones that contain fractures may seal the petroleum trap in some areas, but thet may leak in others (Rawling et al., 2001). The heterogeneous structures of fault damage zones can strongly influence hydrologic properties in a hydrocarbon basin, including the (1) fault core thickness and gouge grain size. Eichhubl et al. (2005) present clay (or gouge) smear within the fault core and increasingly localized deformation of the clay component at a sandstone/shale bed interface. Such a clay smear is commonly used to describe a collection of fault gouges acting as a capillary seal preventing cross-fault flow (Eichhubl et al., 2005; Vrolijk et al., 2016). Seals could fail due to high-permeability "hydraulic holes" (Caine and Minor, 2009). (2) The fracture network distribution — fault propagation leads to the creation of a cloud of microfractures as a result of stress concentration at the fault tip. These fractures are distributed and connected within the damage zones, providing primary fluid conduits in the subsurface (Caine et al., 1996; Faulkner et al., 2010). (3) The

[1]China University of Petroleum (Beijing), State Key Laboratory of Petroleum Resources and Prospecting, Beijing 102249, China and China University of Petroleum (Beijing), College of Geosciences, Beijing 102249, China. E-mail: zonghuliao@163.com (corresponding author); huayaozou@cup.edu.cn.

[2]China University of Petroleum (Beijing), College of Geosciences, Beijing 102249, China. E-mail: whalen_ch@outlook.com.

[3]University of Oklahoma, School of Geology and Geophysics, Norman, Oklahoma 73072, USA. E-mail: xfchen0515@gmail.com.

[4]China University of Petroleum(East China), School of Geosciences, Qingdao, Shandong 266555, China. E-mail: haofang@upc.edu.cn.

Manuscript received by the Editor 27 June 2019; revised manuscript received 13 September 2019; published ahead of production 2 April 2020. This paper appears in *Interpretation*, Vol. 8, No. 4 (November 2020); p. 1–11, 8 FIGS.

http://dx.doi.org/10.1190/INT-2019-0107.1.

lithification of protolith rocks — he lithification could be used to predict the juxtapositions for a given fault geometry (Knipe, 1997) and evaluate the sealing potential of the fault (Peacock et al., 2000). Brittle lithified sediments usually enhance horizontal flow in fault damage zones. However, faulting within poorly lithified sediments has less potential to act as vertical and horizontal flow conduits (Rawling et al., 2001). The difference is due to whether there is an absence of macroscopic fractures associated with fault damage zones.

Fractures surrounding faults are usually investigated by outcrop analyses on the surface (Mitchell and Faulkner, 2009; Sagy et al., 2001; Wilson et al., 2003; Savage and Brodsky, 2011). The fractures tend to locate near the fault core, and the fracture density decreases outward from the fault core. The damage zone extends outward from the fault core to a point where the structure density approximately equals the background density. Such observational outcrop studies are difficult for subsurface fracture characterizations because direct subsurface observation is costly and is only in areas around the wellbore. Peng et al. (2003) and Xu et al. (2012) use synthetic-wave and real seismic-wave events to characterize subsurface damage zones indirectly. The variation of seismicity rate is applied for damage zones in the Elsinore-Temecula segment of the southern San Andreas Fault system (Powers and Jordan, 2010), and high-resolution earthquake locations are used to evaluate the damage zone in the L'Aquila normal fault, Italy (Valoroso et al., 2014). They find a damage zone with damage intensity decaying from the fault core outward, agreeing with field observations. However, the poor seismic resolution limited the characterization to only approximately the kilometer scale. With the advance of seismic survey in petroleum industry, seismic attributes with good resolution is used to characterize fault and its surrounding deformation by inferring from seismic disturbance volume indirectly (Chopra and Marfurt, 2007; Iacopini and Butler, 2011; Iacopini et al., 2012; Qi et al., 2014, Liao et al., 2019). However, the properties of subsurface damage zones, including fractures, superposition architecture, and regional distribution, have been poorly studied and discussed.

The growing need for fracture evaluation extends from mineralized veins to shale play and tight gas reservoirs. In this study, we focus on fractures in tight sandstone within the Xujiahe Formation in the Sichuan Basin, China. In general, a tight sandstone reservoir means a reservoir with permeability less than 0.1 mD and porosity less than 10%. In the Xujiahe Formation, the matrix porosity is less than 5%, and the permeability is less than 0.05 mD. Tight gas usually cannot be produced naturally without drilling intervention, e.g., hydrofracturing and horizontal drilling (Zou et al., 2012). In this case, however, high production from several pioneering wells in the tight sandstone Xujiahe Formation exhibited greater hydrocarbon potential than expected, suggesting that the permeability is controlled by the presence of fractures rather than low-permeability sandstone matrix. The essential characteristics of the tight gas reservoir in Sichuan Basin include but not limited to the (1) proximity relation of coal sources and reservoir rocks (Wang et al., 2013; Qin et al., 2018), (2) overpressure in tight sandstone reservoir, and (3) unique migration and accumulation mechanisms coupling fractures and overpressure (Tingay et al., 2009; Hao et al., 2015). All these features are related to fractures; therefore, the Xujiahe Formation provides an ideal case for studying the fractured tight gas reservoir. This study displays the damage zones of a subsurface sandstone tight gas reservoir in northeast Sichuan, China at multiple scales: from kilometer scale using seismic attributes toward outcrop and image logging observations and down to microfracture characterizations from thin sections. The results indicate that the fractures within damage zones have the potential to act as reservoir storage space and horizontal-flow conduits over a regional scale. We further illustrate the relation between damage zones and overpressure, and the main factors controlling gas migration and accumulation. The result could provide insights for the next exploration deployment in tight sandstones.

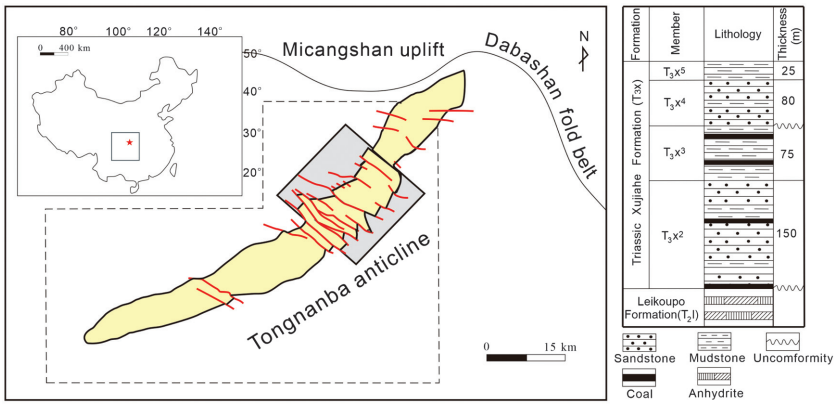

Figure 1. (a) Study area within the Xujiahe Formation and (b) strata column in the middle of the Tongnanba fold in northeast Sichuan, China. The red lines are generalized faults, and not all faults are shown.

Geologic setting

The Tongnanba anticline is one of the superimposed basins located northeast of the Sichuan Basin, China (Figure 1a). Its evolution is controlled by the Micangshan thrust in the northwest, Dabashan thrust-fold belt in the northeast, and the Longmenshan fault belt far in the west. The study focuses on the middle segment of the Tongnanba fold within the second member of the Upper Triassic Xujiahe Formation (T_3x). It is an anticlinal fold striking northeast–southwest, structurally consistent with the two seg-

ments not covered by the data in the study: one segment in the northeast and the other one in the southwest. The axis of the Tongnanba anticline is tilted from high in the southwest to low in the northeast, with both limbs dipping gently. It is a large anticline with approximately 12.2 km in width and 80 km in length, among which a sequence of northwest-striking reverse faults developed with subfolds (the red lines in Figure 1a). By analyzing the evolution of the superposition system of folds and faults, two stages of significant tectonic movements could be recognized (Dai et al., 2013; Li et al., 2016). In the first stage, the Tongnanba anticline formed by northwest–southeast compression in the Middle-Late Jurassic Micangshan deformation. In a later stage, Tongnanba anticline is further ruptured by the northeast–southwest compression from the Dabashan thrust in the Himalayan orogeny, resulting in the formation of subfolds and reverse faults. Details of the associated deformation are discussed later.

There are three major gas-bearing formations in the study area (Wang et al., 2013; Qin et al., 2018), including the Upper Permian Changxing Formation (P_2c), the Lower Triassic Feixianguan Formation (T_1f), and the Upper Triassic Xujiahe Formation (T_3x) (this study). Our focus here is the Xujiahe Formation, which is a set of tight continental sandstone interbedded with gas-rich coal seams and silty mudstone that could be further divided into following five bottom-top members (Figure 1b): (1) The first member is a 40 m thick silty mudstone. A thick layer of anhydrite from the Leikoupo Formation lays below the first member. (2) The second member is composed of 200 m thick sandstone under overpressure and two coal seams in the lower part, which is the focus of this study. The coal seams are rich in gas and are source rocks for commercial explorations. (3) The third member is a 100 m thick silty mudstone that acts as a direct seal for the tight sandstone of the second member. (4) The fourth member is a 100 m thick sandstone. (5) The fifth member is a 50 m thick silty mudstone. The second member of tight sandstone of the Xujiahe Formation is the principal gas-producing layer, whereas the fourth member is also of great potential but will not be discussed here. Because the second member tight sandstone has ultralow porosity (<5%,) and ultralow permeability (<0.1 mD), the high production wells in Tongnanba lead to significant interests in studying the factors controlling the gas migration and accumulations (Li et al., 2016; Yue et al., 2018).

Microfractures in tight sandstone

Previous work reveals that microfractures strongly influence rock strength, elastic wave velocities, and permeability (Kranz, 1983; Anders et al., 2013). Here, we present thin section images of the samples taken from tight sandstone of the second Xujiahe Formation, with abundant microfractures (Figure 2). The present tight sandstone has three facies, a pure quartz sandstone with substantial quartz overgrowth as evidenced by the low grain boundary contrast (Figure 2a–2c), a sandstone with chlorite coating (the thick dark lines bounding the grain boundaries in Figure 2d–2f), and a clastic sandstone with muddy fillings (Figure 2g–2i). No appreciable void spaces can be visually observed in these images, indicating very low porosity in the sandstone matrix. The sand grain texture has a strong influence on the microfractures because most of the microfractures tend to follow grain boundaries (Figure 2a, 2b, 2d, 2f, and 2h). Besides the predominant intergranular fractures, transgranular fractures also exist, cutting across hosting grains and straightening the fracture traces (Figure 2c, 2g, and 2i). Considering the multistage tectonic histories in the area (Dai et al., 2013; Li et al., 2016), these microfractures are likely developed subcritically under relatively small driving stresses (Olson et al., 2009; Chen et al., 2017, 2019) such as episodes of overpressure caused by gas expulsion during the Jurassic, local tensile stress by Tongnanba folding during the Jurassic and the Early Cretaceous, and unloading by basin uplift during the Later Cretaceous.

The tight nature of the sandstone is further manifested in the petrophysical measurements from a total of 58 core samples, laid out as compared with other tight sandstone gas reservoirs around the world (Figure 3). The porosity is generally fewer than 2% for the quartz sandstone and the sandstone with chlorite-coat, and 2%–5% for the sandstone mixed with muddy grains, giving an average porosity of 1% for the Tongnanba sandstone reservoir (Figure 3a), which is significantly lower than others (Figure 3a). Not only with low porosity, but the permeability of the present sandstone is also low as compared with other tight sandstone gas reservoirs, with the permeability distributed mainly between 0.01 and 0.05 mD (Figure 3b). Water saturation (e.g., 60% in this case) is higher than others. The wider scatter of the permeability range than the less scattered porosity range (Figure 3a and 3b) suggests that fractures provide significant permeability than porosity in the tight sandstone.

Macrofractures in fault damage zones

At the outcrop scale, fractures further develop into joints (Figure 4a and 4b). These fractures extend vertically across the bedding layers, forming multiple sets of fractures cross linked to a fracture network as commonly seen in brittle formations of carbonates and shales (Gale et al., 2007; Guerriero et al., 2010). The spacing between fractures can be as narrow as a few centimeters (Figure 4a) but can also be as wide as approximately meters (Figure 4b). The high angle fracture sets observed in logging image (Figure 4d and 4e) is consistent with outcrop observations. The vertically extending fractures mostly end into intact mudstone/siltstone, together with the horizontally extending fractures, significantly enhancing fluid flow properties within the layer. The formation of joint network indicates that the fractures were mainly developed subcritically (Pollard and Aydin, 1988; Olson et al., 2009), which

further suggests that the coupled mechanical (rock strength, elastic properties) and chemical (stress corrosion, dissolution-precipitation) effects contribute to the fracture system development (Atkinson, 1984; Chen et al., 2017, 2019).

Damage zones distribution by seismic attributes

The basin is majorly composed of a large anticlinal Tongnanba fold (Figure 5a) that is cross-cut by a series of reverse faults into isolated subfolds (Figure 2a). As observed in microfractures from core samples and fracture networks from outcrops and image logging, the distribution of fracture bearing damage zones is critical for understanding the migration conduits on a basin scale. It is expected that the area is densely fractured due to the superposition of multiple sequences of tectonic movements and the associated stress localizations around the anticline structure (Reches, 1988; Staples, 2011; Liao et al., 2019). We use seismic attributes calculated from the 3D seismic reflection data to image the seismic deformations within the Xujiahe Formation (Marfurt and Rich, 2010; Iacopini et al., 2012; Botter et al., 2016, 2017; Liao et al., 2019).

We compute variance and enhance the variance image based on the ant-tracking technique. The coherence attribute is defined as the energy of the coherent part of seismic traces divided by the average acoustic energy of the input seismic traces (Chopra and Marfurt, 2007). We applied statistical variance, a reversed version of the coherence described by Gerztenkorn and Marfurt (1999), with the high variance values equivalent to faults. Figure 5b shows the variance image computed from Petrel, which is a patented algorithm. The ant-tracking attrib-

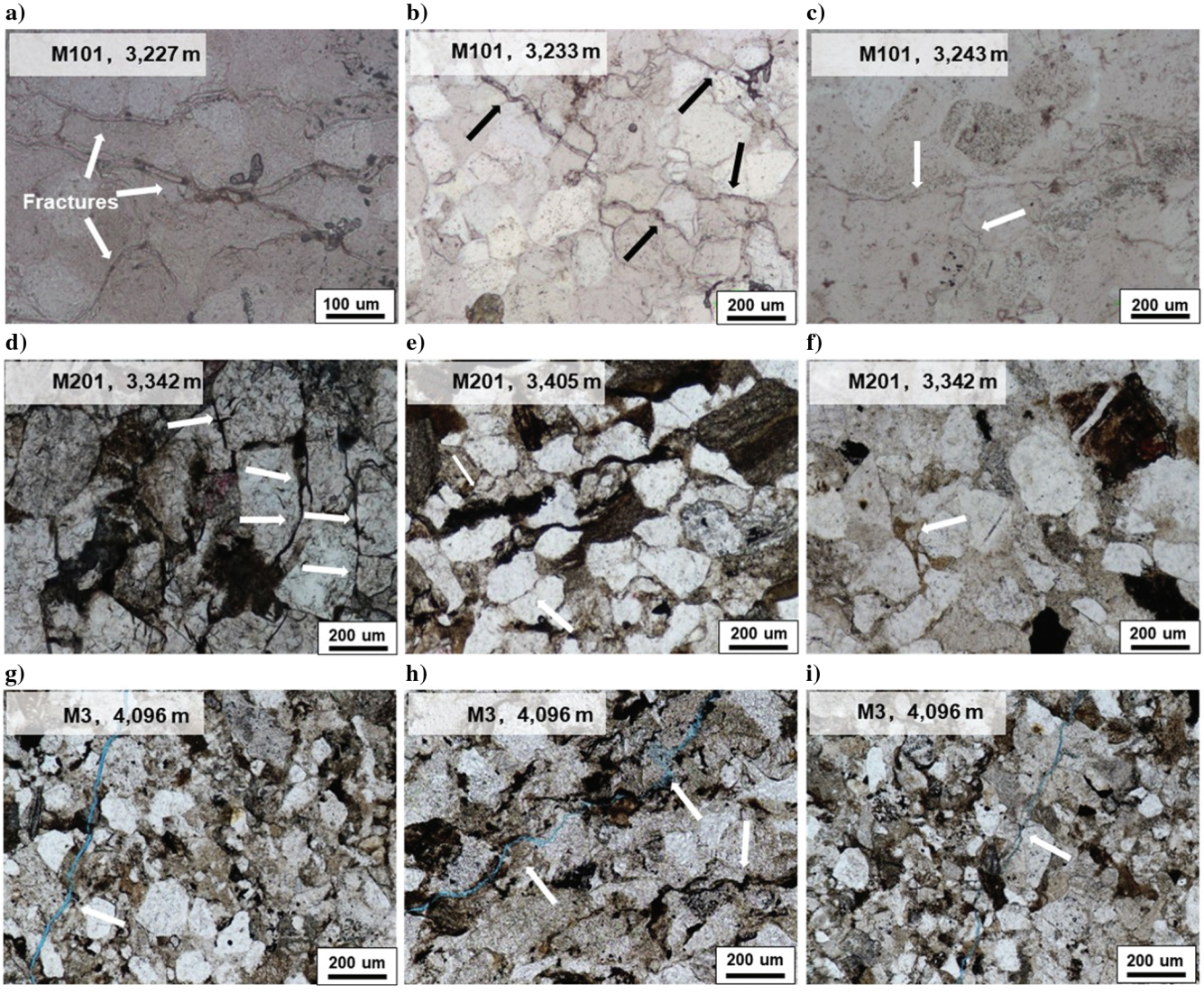

Figure 2. Thin section imaging of microfractures from three wells in the tight sandstone reservoir under plane-polarized light. (a-c) Quartz-sandstone with multiple opening-mode microfractures (arrows) from well M101. Substantial quartz overgrowth is evidenced by the low grain boundary contrast. (d-f) Microfractures in the sandstone with chlorite-film (dark intergranular marks) coating the grains from well M201. (g-i) Microfractures (blue lines) in a quartz-rich clastic sandstone from well M3. Muddy fillings (dark areas) reside the intergranular spacing.

ute is an algorithm adapted from the ant-colony systems to capture trends in noisy data of the other attributes in three dimensions. This approach enhances the structure of discontinuities and filters nonstructural features (Jansen, 2005). It is a statistical edge enhancement tool, allowing the interpreter to better characterize faults in the seismic data. It is important to note that ant tracking may produce artificial faults, e.g., connecting inosculating fault segments, or misinterpretation of footprints (Jansen, 2005).

The variance and ant-tracking attributes are computed along the top of the Xujiahe Formation, and our observations include the following two parts: (1) two large areas with high variance values distributed in the upper left and lower right parts (Figure 5b), which are transition areas of limbs and envelope layers, and (2) distinguishable strips of high variance trending north–south (red in Figure 5b). The structures of the strips are further illustrated in the ant-tracking attribute map, where additional small faults are indicated by the red arrows (Figure 5c). These strips are interpreted as fault damage zones formed due to compression from the Dabashan thrust in the northeast (Figure 2a) during the Himalayan orogeny. These strips strike between 335° and 345°. We picked up six major damage zones of reverse faults (Figure 5d) divided into two groups based on fault length. (1) The long faults that cross the Tongnanba fold, including F1, F3, and F6 with fault lengths ranging from 12 to 20 km. These long faults consist of two segments slightly separated by axis-normal subfaults on the Tongnanba fold hinge, where dense fractures are inferred owing to the superposition of folding flexures and subfaults. (2) The short faults that mostly appear on the north limb of the Tongnanba fold,

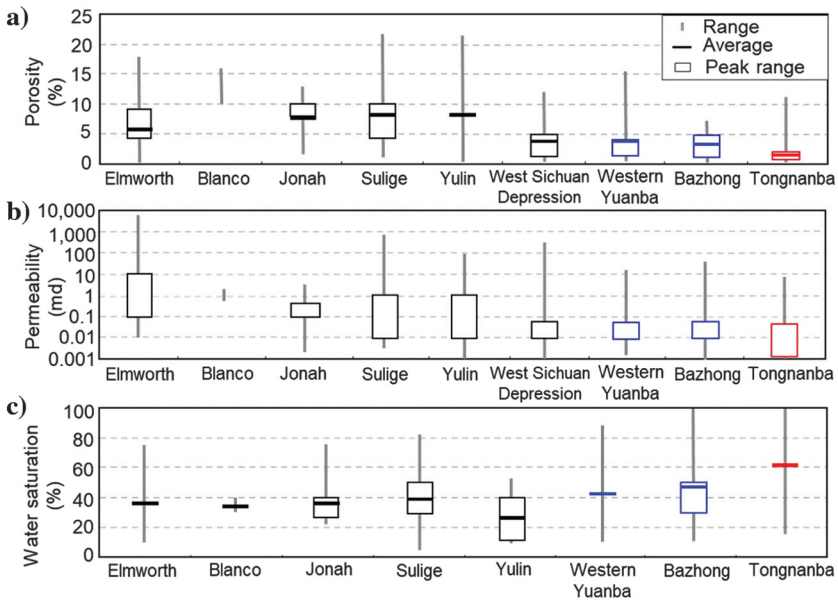

Figure 3. Comparison of the rock properties of tight sandstone in the Xujiahe Formation to the other tight sandstone in the world, including (a) porosity, (b) permeability, and (c) water saturation. The red is data in the Tongnanba, the blue is data in the Sichuan Basin, and the black is referred to data (Zou et al., 2012; Song et al., 2018).

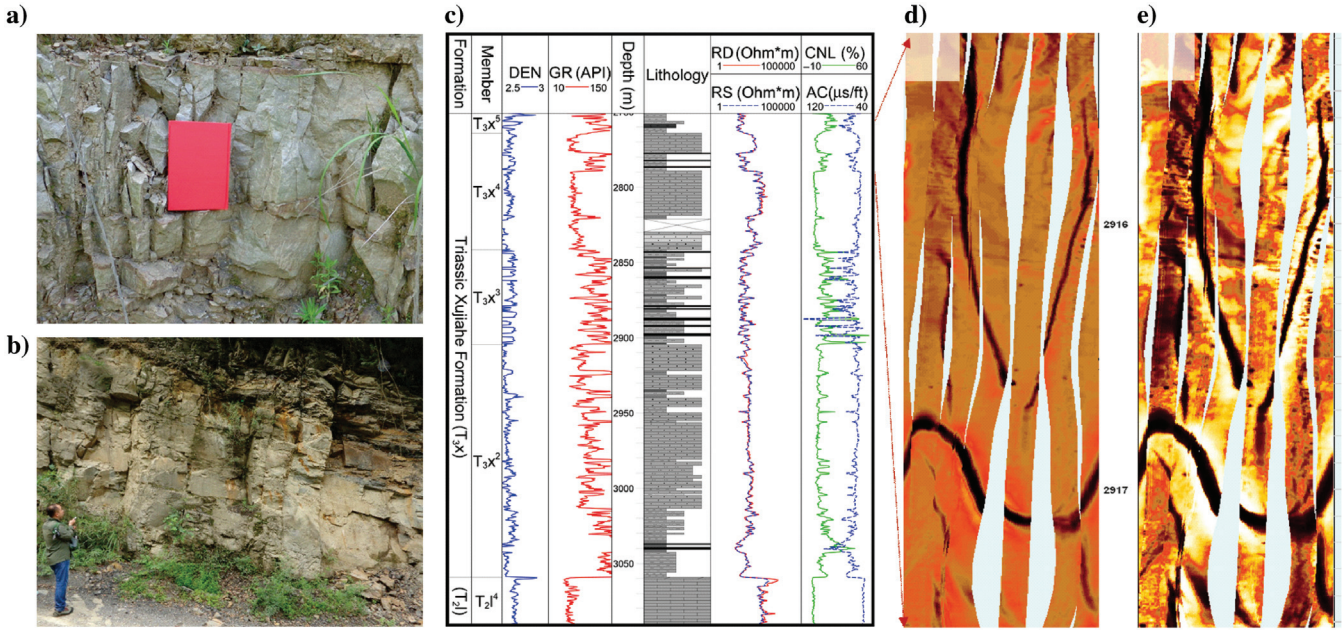

Figure 4. Fractures at (a and b) the outcrop (20 km north of the study area) of the second member of the Xujiahe Formation and (c) stratigraphy with logging data, and (d and e) imaging log (well M103, 2916 m in depth).

including F2, F4, and F5 with lengths approximately 8–10 km.

Furthermore, to investigate the internal structure of the damage zones, we crop a cube of the data set from the Tongnanba fold (the black dashed box in Figure 5b and 5c) containing the sandstone Xujiahe Formation. Figure 6a presents a 3D seismic amplitude data corendered with variance attribute (the color bar differs from Figure 5b for clarity). The amplitude generally shows continuous reflectors and defines the subanticlines of the Xujiahe Formation in gray. The yellow-red color clusters (F1, F2, and F3 in Figure 6a) are high-seismic-variance anomalies that can be readily interpreted as fracture networks within fault damage zones (Chopra and Marfurt, 2007; Li et al., 2016; Liao et al., 2019). It sometimes is defined as a seismic disturbance zone (Iacopini et al., 2012) as a result of the cumulative effects of faults and fractures. The enhanced discontinuity (Figure 6b) by amplitude data corendered with ant tracking presents the potential slip surfaces of the reverse faults. This indicates that the faults may be segmented or inosculated vertically. Figure 6c presents the distribution patterns of damage zones, including multilayers of anhydrite, sandstone, and mudstone/siltstone. The thickness of these damage zones ranges from 100 to 1500 m (Figure 6c). The two wells, M101 and M103, are located precisely by the side of a most substantial reverse fault, F3 (Figures 5b, 5d, and 6a). It is likely that the damage zones (Figures 5d and 6c) inferred from the disturbed seismic signals represent a volume of densely developed fractures as observed in the field (Figures 2, 4c, and 4d), impacting the migration and accumulations of gas.

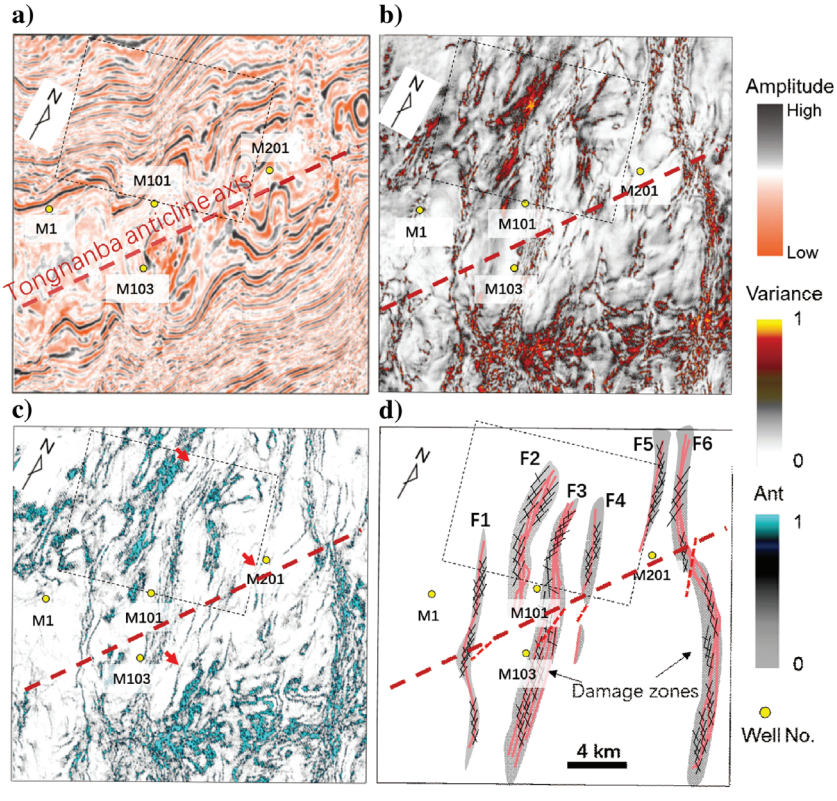

Figure 5. (a) Time slice map of seismic amplitude and seismic attributes of coherences calculated for tight sandstone in the second member of Xujiahe Formation in the study area, including (b) variance and (c) ant tracking. (d) The interpretation of damage zones on the crest of the Tongnanba fold. Note that the red dashed line in (a) is the Tongnanba fold axis and the red arrows in (c) indicate fault lineaments. Locations of wells marked. The area in the black dashed box is to present later.

Implication and discussions

Fractures, damage zones, and gas migration

Fracture is a significant geologic factor controlling shale plays (Decker et al., 1992; Hill and Nelson, 2000). Higher gas productivity is often linked to fracture zones, whereas there is low or no gas production to the poorly deformed area. A densely developed fracture network will significantly increase gas production in a low-porosity reservoir (Hill and Nelson, 2000). In the present case, commercial gas production is obtained in the middle part of the Tongnanba fold crest where fractures densely developed. The fractures (Figures 2 and 4) form subcritically during multiple stages of tectonic movements assisted by the episodes of overpressure, which we argue supply the large storage volume for free gas and desorption gas in an originally tight and less permeable sandstone (Curtis, 2002). In addition, fractures within damage zones further provide major migration channels (Figures 5d and 6c), including three distinct stages based on geochemical and geostructural data (Li et al., 2016; Song et al., 2018).

1) Late Triassic to Middle Jurassic (208–160 Ma): the early stage of gas accumulation in the lithologic reservoir. Gas generation occurs from the source rocks of the Xujiahe Formation in the Tongnanba area at the end of the Late Triassic Xujiahe Formation, but at this time, the Tongnanba anticline has not yet formed and the horizontal stratum is stable with few faults. A considerable amount of gas is expulsed (Wang et al., 2013; Li et al., 2016; Song et al., 2018) into the surrounding sandstone of the second member through subcritical microfractures in the Middle Jurassic. It is lithologic-controlled reservoirs without much interaction of fractures or faults at this stage.
2) Late Jurassic to Early Cretaceous (160–100 Ma): the intermediate stage of gas accumulation in the tectonic-lithologic reservoir. Under the influence of the movement of the Yanshan Mountains, the thrusting and

extrusion of the Dabashan structural belt caused the initial formation of the Tongnanba anticline and formed a large number of fold-controlled tensile fractures. A significant amount of fractures formed, and the gas generated by the Xujiahe Formation coal seams starts to migrate and accumulate in the high structural area (the subhorizontal red arrows in Figure 7). The lithologic-controlled reservoir is transformed into a tectonic-lithologic gas reservoir.

3) Late Cretaceous to the present (approximately 100 Ma): the late stage of gas redistribution and reservoir adjustment. Since the late Cretaceous, due to the influence of the Yanshan Movement and the Xishan Movement, the northeastern Sichuan region has been dramatically uplifted and the source rocks of the Xujiahe Formation have ceased to produce hydrocarbons. The Tongnanba anticline is further uplifted and deformed with a large number of faults and fractures through the Permian and Triassic. The unloading and compression turn damage zones to the mature stage during the reservoir transformation, providing conduits for gas flowing upward. The favored area, e.g., the crest of the anticlinal fold (well M101), is charged by the surrounding gas and is enriched by mixing the potential marine gas migrated through damage zones (the red arrows in F3, Figure 7). The gas is accumulated in the anticlinal top and damage zones with dense fractures in tight sandstone, forming the distribution characteristics of today's gas reservoirs. A certain amount of gas has been leaked upward to the fourth member through the damage zones, e.g., F3.

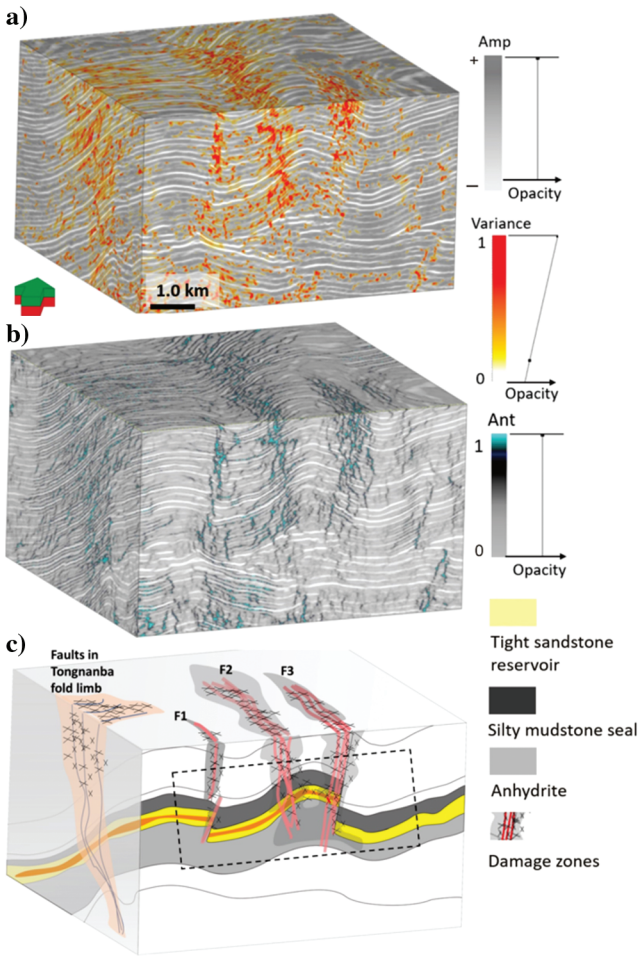

Figure 6. The 3D seismic volume visualizations for the damage zones of the fold-thrust structure in Tongnanba fold. (a) Seismic cube of amplitude corendered with variance. The red/yellow scale gradational color has been adopted to highlight major discontinuities defined as damage zones. (b) Seismic cube of amplitude corendered with ant-tracking calculated from the amplitude. (c) Structure interpretation model of the study area with fault damage zones and major strata of the Xujiahe sandstone/mudstone as well as the Leikoupo anhydrite. Note that the damage zones are composed of red lines (as the fault core) surrounded with a gray area (as the damage zones). The damage zones on the left of the figure in light orange are the fault zones in Tongnanba fold limb that is not discussed here. The black dashed box is the study area for Figure 7.

Coupling between fractures and overpressure

The tight sandstone in the Tongnanba area has a high degree of consolidation (Figure 2) with poor reservoir petrophysical properties (Figure 3) (low porosity and low permeability) and substantial structural heterogeneity (Figures 5–7). Therefore, faults and fractures act as effective channels for the migration, accumulation, and dissipation of gas. In the Tongnanba area, the drilling positions (e.g., wells Ma 101 and Ma 103; Figure 5) are in the Tongnanba anticline core, which is at a structural high point and is conducive to the accumulation of gas. We argue that the folding flexures provide the conductivity in the crest of the Tongnanba fold aided by the fractures in the damage zones of F2 and F3. The in situ pressure coefficients (approximately 1.5, Figure 8) indicate that the reservoir of the Xujiahe Formation is under overpressure. The overpressure in the lower formations, e.g., the Jurassic J1, J2 Formations in Figure 8, indicates excellent sealing by the mudstone interlayers in this area. In the current reservoir of the Xujiahe Formation, due to the complexity of geo-

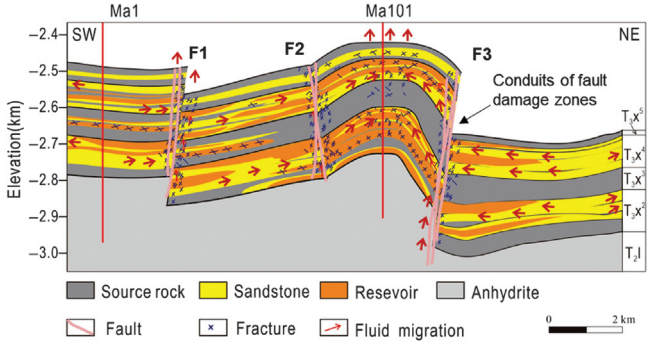

Figure 7. Model of conduits for gas migration and accumulation in the Tongnanba fold. The location of wells Ma101 and Ma1 is shown.

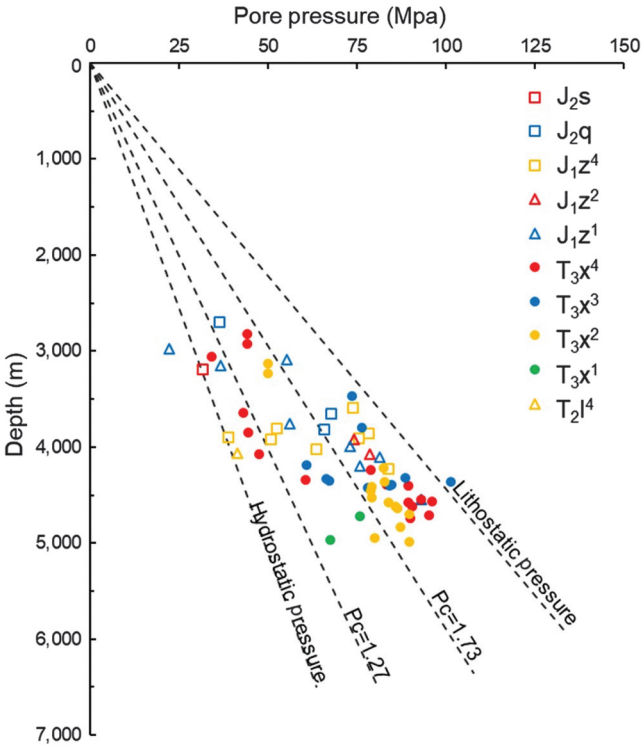

Figure 8. Measured pore pressure versus depth in the Tongnanba area, Sichuan Basin (adapted from Song et al., 2018). The red dots are well data from Xujiahe Formation, Triassic (T), whereas the others are from Jurassic formations (J).

logic conditions, the overpressure results from a combination of mechanisms, including diagenesis and gas generation, compaction, and tectonic compression (Dai et al., 2013; Li et al., 2016).

The coupling effect between fracture and overpressure is mainly reflected in three aspects. (1) The overpressure in the reservoir increases the potential for the development and preserve of opening mode microfractures. This increases the storage volume and permeability significantly (Wibberley and Shimamoto, 2005; Faulkner et al., 2010; Lockner et al., 2011; Cavailhes et al., 2013). (2) Rupture of the formation or opening of the fracture network leads to the release of overpressure. Thus, overpressure is challenging to sustain during a long geologic time (Tingay et al., 2009; Hao et al., 2015). Hydraulic fractures were found to reduce the overpressure in the Yuanba area, south of the study area (Li et al., 2016). (3) The fracture networks provide conduits for redistribution of overpressure compartments (Hao et al., 2015; Song et al., 2018). The overpressured gas migrates through the fracture network to the higher structures, forming a high-pressure and high-yield gas reservoir. Industrial gas flows (e.g., well M101) were obtained in the crest of the Tongnanba fold surrounded by damage zones of F2 and F3, which is a favored structurally high zone of accumulated gas with a high fracture density. Wells Ma102 and M3 near the fault damage zones also obtained industrial gas flow, whereas well M2 slightly away from the fault zone did not receive industrial gas flow. This confirms that the enrichment and high yield of gas need to be based on the development of fractures. The associated core samples from the Xujiahe Formation display unfilled and active fractures (Figures 2 and 4), which we argue provide the large fracture-based volume for gas storage within the low-porosity tight sandstone, particularly under overpressure conditions.

Conclusion

In this study, we show that seismic attributes could be used to characterize the structure and distribution of fault damage zones in the subsurface, taking the tight sandstone in the northeast Sichuan Basin as an example. We have demonstrated the characteristics of the microfractures and macrofractures within these damage zones, which we argue provide ample potential volumetric storage space for gas and primary migration conduits. This approach and data extend the reliable evaluation of fault damage zones on a regional scale that significantly controls the basin-wide migration and distribution of gas. Finally, the coupling effect between fractures and overpressure in tight sandstone provide insights for understanding the accumulation mechanisms of tight gas, which could also extend to CO_2 sequestration.

Acknowledgments

The authors would like to thank the three anonymous reviewers, Sinopec China for providing a license to their 3D seismic data, and the sponsors of the Attribute Assisted Seismic Processing and Interpretation, University of Oklahoma. Support funds were provided by the Strategic Priority Research Program of the Chinese Academy of Sciences XDA14010306 and the National Natural Science Foundation of China no. U1663203 and no. 41604036.

Data and materials availability

Data associated with this research are available and can be obtained by contacting the corresponding author.

References

Anders, M. H., J. R. Schneider, C. H. Scholz, and S. Losh, 2013, Mode I microfracturing and fluid flow in damage zones: The key to distinguishing faults from slides: Journal of Structural Geology, **48**, 113–125, doi: 10.1016/j.jsg.2012.11.010.

Atkinson, B. K., 1984, Subcritical crack growth in geological materials: Journal of Geophysical Research: Solid Earth, **89**, 4077–4114, doi: 10.1029/JB089iB06p04077.

Botter, C., N. Cardozo, S. Hardy, I. Lecomte, G. Paton, and A. Escalona, 2016, Seismic characterization of fault damage in 3D using mechanical and seismic modeling: Marine and Petroleum Geology, **77**, 973–990, doi: 10.1016/j.marpetgeo.2016.08.002.

Botter, C., N. Cardozo, D. Qu, J. Tveranger, and D. Kolyukhin, 2017, Seismic characterization of fault facies models: Interpretation, **5**, no. 4, SP9–SP26, doi: 10.1190/INT-2016-0226.1.

Busetti, S., K. Mish, P. Hennings, and Z. Reches, 2012, Damage and plastic deformation of reservoir rocks — Part 2: Propagation of a hydraulic fracture: AAPG Bulletin, **96**, 1711–1732, doi: 10.1306/02011211011.

Caine, J. S., J. P. Evans, and C. B. Forster, 1996, Fault zone architecture and permeability structure: Geology, **24**, 1025–1028, doi: 10.1130/0091-7613(1996)024<1025:FZAAPS>2.3.CO;2.

Caine, J. S., and S. A. Minor, 2009, Structural and geochemical characteristics of faulted sediments and inferences on the role of water in deformation, Rio Grande Rift, New Mexico: Geological Society of America Bulletin, **121**, 1325–1340, doi: 10.1130/B26164.1.

Cavailhes, T., R. Soliva, P. Labaume, C. Wibberley, J.-P. Sizun, C. Gout, D. Charpentier, A. Chauvet, B. Scalabrino, and M. Buatier, 2013, Phyllosilicates formation in faults rocks: Implications for dormant fault-sealing potential and fault strength in the upper crust: Geophysical Research Letters, **40**, 4272–4278, doi: 10.1002/grl.50829.

Chen, X., P. Eichhubl, and J. E. Olson, 2017, Effect of water on critical and subcritical fracture properties of Woodford shale: Journal of Geophysical Research: Solid Earth, **122**, 2736–2750, doi: 10.1002/2016JB013708.

Chen, X., P. Eichhubl, J. E. Olson, and T. A. Dewers, 2019, Effect of water on fracture mechanical properties of shales: Journal of Geophysical Research: Solid Earth, **124**, 2428–2444, doi: 10.1029/2018JB016479.

Chester, F. M., and J. M. Logan, 1986, Implications for mechanical properties of brittle faults from observations of the Punchbowl Fault Zone, California: Pure and Applied Geophysics, **124**, 79–106, doi: 10.1007/BF00875720.

Chopra, S., and K. J. Marfurt, 2007, Seismic attributes for prospect identification and reservoir characterization: SEG Geophysical Developments Series No. 11.

Curtis, J. B., 2002, Fractured shale-gas systems: AAPG Bulletin, **86**, 1921–1938, doi: 10.1306/61EEDDBE-173E-11D7-8645000102C1865D.

Dai, J., F. Liao, and Y. Ni, 2013, Discussions on the gas source of the Triassic Xujiahe Formation tight sandstone gas reservoirs in Yuanba and Tongnanba, Sichuan Basin: An answer to Yin Feng et al.: Petroleum Exploration and Development, **40**, 268–275, doi: 10.1016/S1876-3804(13)60033-6.

Decker, A. D., J. M. Coates, and D. E. Wicks, 1992, Stratigraphy, gas occurrence, formation evaluation and fracture characterization of the Antrim shale, Michigan Basin: GRI Topical Report, No. GRI-92/0258, p. 153.

Eichhubl, P., P. S. D'Onfro, A. Aydin, J. Waters, and D. K. McCarty, 2005, Structure, petrophysics, and diagenesis of shale entrained along a normal fault at Black Diamond Mines, California — Implications for fault seal: AAPG Bulletin, **89**, 1113–1137, doi: 10.1306/04220504099.

Ellis, M. A., S. E. Laubach, P. Eichhubl, J. E. Olson, and P. Hargrove, 2012, Fracture development and diagenesis of Torridon Group Applecross Formation, near An Teallach, NW Scotland: Millennia of brittle deformation resilience: Journal of the Geological Society, **169**, 297–310, doi: 10.1144/0016-76492011-086.

Faulkner, D. R., C. A. L. Jackson, R. J. Lunn, R. W. Schlische, Z. K. Shipton, C. A. J. Wibberley, and M. O. Withjack, 2010, A review of recent developments concerning the structure, mechanics and fluid flow properties of fault zones: Journal of Structural Geology, **32**, 1557–1575, doi: 10.1016/j.jsg.2010.06.009.

Gale, J. F. W., R. M. Reed, and J. Holder, 2007, Natural fractures in the Barnett Shale and their importance for hydraulic fracture treatments: AAPG Bulletin, **91**, 603–622, doi: 10.1306/11010606061.

Gerztenkorn, A., and K. J. Marfurt, 1999, Eigenstructure based coherence computations as an aid to 3-D structural and stratigraphic mapping: Geophysics, **64**, 1468–1479, doi: 10.1190/1.1444651.

Guerriero, V., A. Iannace, S. Mazzoli, M. Parente, S. Vitale, and M. Giorgioni, 2010, Quantifying uncertainties in multi-scale studies of fractured reservoir analogues: Implemented statistical analysis of scan line data from carbonate rocks: Journal of Structural Geology, **32**, 1271–1278, doi: 10.1016/j.jsg.2009.04.016.

Hao, F., W. Zhu, H. Zou, and P. Li, 2015, Factors controlling petroleum accumulation and leakage in overpressured reservoirs: AAPG Bulletin, **99**, 831–858, doi: 10.1306/01021514145.

Hill, G., and C. R. Nelson, 2000, Reservoir properties of the Upper Cretaceous Lewis Shale, a new natural gas play in the San Juan Basin: AAPG Bulletin, **84**, 1240.

Iacopini, D., and R. W. H. Butler, 2011, Imaging deformation in submarine thrust belts using seismic attributes: Earth and Planetary Science Letters, **302**, 414–422, doi: 10.1016/j.epsl.2010.12.041.

Iacopini, D., R. W. H. Butler, and S. Purves, 2012, Seismic imaging of thrust faults and structural damage visualization workflow for deepwater thrust belts: First Break, **30**, 39–46.

Jansen, K., 2005, Seismic investigation of wrench faulting and fracturing at Rulison field: M.S. thesis, Colorado School of Mines, Golden, CO, USA.

Katz, O., Z. Reches, and G. Baer, 2003, Faults and their associated host rock deformation — Part 1: Structure of small faults in a quartz-syenite body, southern Israel: Journal of Structural Geology, **25**, 1675–1689, doi: 10.1016/S0191-8141(03)00011-7.

Knipe, R. J., 1997, Juxtaposition and seal diagrams to help analyze fault seals in hydrocarbon reservoirs: AAPG Bulletin, **81**, 187–195, doi: 10.1306/522B42DF-1727-11D7-8645000102C1865D.

Kranz, R. L., 1983, Microcracks in rocks: A review: Tectonophysics, **100**, 449–480, doi: 10.1016/0040-1951(83)90198-1.

Laubach, S. E., P. Eichhubl, P. Hargrove, M. A. Ellis, and J. N. Hooker, 2014, Fault core and damage zone fracture attributes vary along strike owing to interaction of fracture growth, quartz accumulation, and differing sandstone composition: Journal of Structural Geology, **68**, 207–226, doi: 10.1016/j.jsg.2014.08.007.

Li, J., D. Hu, H. Zou, X. Shang, H. Ren, and L. Wang, 2016, Coupling relationship between reservoir diagenesis and gas accumulation in Xujiahe Formation of Yuanba — Tongnanba area, Sichuan Basin, China, Journal of Natural Gas Geoscience, **1**, 335–352, doi: 10.1016/j.jnggs.2016.11.003.

Liao, Z., H. Liu, B. M. Carpenter, K. J. Marfurt, and Z. Reches, 2019, Analysis of fault damage-zones by using 3D seismic coherence in Anadarko Basin, Oklahoma: AAPG Bulletin, **103**, 1771–1785, doi: 10.1306/1219181413417207.

Lockner, D., C. Morrow, D. Moore, and H. Stephen, 2011, Low strength of deep San Andreas fault gouge from SAFOD core: Nature, **472**, 82–85, doi: 10.1038/nature09927.

Marfurt, K. J., and J. Rich, 2010, Beyond curvature-volumetric estimation of reflector rotation and convergence: 80th Annual International Meeting, SEG, Expanded Abstracts, 1467–1472, doi: 10.1190/1.3513118.

Mitchell, T. M., and D. R. Faulkner, 2009, The nature and origin of off fault damage surrounding strike-slip fault zones with a wide range of displacements: A field study from the Atacama fault system, northern Chile: Journal of Structural Geology, **31**, 802–816, doi: 10.1016/j.jsg.2009.05.002.

Mizoguchi, K., and K. Ueta, 2013, Microfractures within the fault damage zone record the history of fault activity: Geophysical Research Letters, **40**, 2023–2027, doi: 10.1002/grl.50469.

Olson, J. E., S. E. Laubach, and R. H. Lander, 2009, Natural fracture characterization in tight gas sandstones: Integrating mechanics and diagenesis: AAPG Bulletin, **93**, 1535–1549, doi: 10.1306/08110909100.

Peacock, D. C. P., R. J. Knipe, and D. J. Sanderson, 2000, Glossary of normal faults: Journal of Structural Geology, **22**, 291–305, doi: 10.1016/S0191-8141(00)80102-9.

Peng, Z., Y. Ben-Zion, A. J. Michael, and L. Zhu, 2003, Quantitative analysis of seismic fault zone waves in the rupture zone of the 1992 Landers, California, earthquake: Evidence for a shallow trapping structure: Geophysical Journal International, **155**, 1021–1041, doi: 10.1111/j.1365-246X.2003.02109.x.

Pollard, D. D., and A. Aydin, 1988, Progress in understanding jointing over the past century: Geological Society of America Bulletin, **100**, 1181–1204, doi: 10.1130/0016-7606(1988)100<1181:PIUJOT>2.3.CO;2.

Powers, P. M., and T. H. Jordan, 2010, Distribution of seismicity across strike-slip faults in California: Journal of Geophysical Research: Solid Earth, **115**, 3040, doi: 10.1029/2008JB006234.

Qi, J., B. Zhang, H. Zhou, and K. J. Marfurt, 2014, Attribute expression of fault-controlled karst — Fort Worth Basin, Texas: A tutorial: Interpretation, **2**, no. 3, SF91–SF110, doi: 10.1190/INT-2013-0188.1.

Qin, S., Y. Zhang, C. Zhao, and Z. Zhou, 2018, Geochemical evidence for in situ accumulation of tight gas in the Xujiahe Formation coal measures in the central Sichuan Basin, China: International Journal of Coal Geology, **196**, 173–184, doi: 10.1016/j.coal.2018.07.009.

Rawling, G. C., L. B. Goodwin, and J. L. Wilson, 2001, Internal architecture, permeability structure, and hydrologic significance of contrasting fault-zone types: Geology, **29**, 43–46, doi: 10.1130/0091-7613(2001)029<0043:IAPSAH>2.0.CO;2.

Reches, Z., 1988, Evolution of fault patterns in clay experiments: Tectonophysics, **145**, 141–156, doi: 10.1016/0040-1951(88)90322-8.

Sagy, A., Z. Reches, and I. Roman, 2001, Dynamic fracturing: Field and experimental observations: Journal of Structural Geology, **23**, 1223–1239, doi: 10.1016/S0191-8141(00)00190-5.

Savage, H. M., and E. E. Brodsky, 2011, Collateral damage: Evolution with displacement of fracture distribution and secondary fault strands in fault damage zones: Journal of Geophysical Research: Solid Earth, **116**, 428–452, doi: 10.1029/2010JB007665.

Song, Y., L. Zhang, D. Luo, S. Yang, F. Hao, and H. Zou, 2018, Characteristics of overpressure regime in compartmentalized overpressured system within tight sandstones, Xujiahe Formation, Yuanba-Tongnanba areas, Sichuan Basin (in Chinese): Petroleum Geology and Experiment, **40**, 613–620.

Staples, E., 2011, Subsurface and experimental analyses of fractures and curvature: M. S. thesis, University of Oklahoma.

Tingay, M. R. P., R. R. Hillis, C. K. Morley, and R. C. King, 2009, Present-day stress and neotectonics of Brunei: Implications for petroleum exploration and production: AAPG Bulletin, **93**, 75–100, doi: 10.1306/08080808031.

Valoroso, L., L. Chiaraluce, and C. Collettini, 2014, Earthquakes and fault zone structure: Geology, **42**, 343–346, doi: 10.1130/G35071.1.

Vrolijk, P. J., J. L. Urai, and M. Kettermann, 2016, Clay smear: Review of mechanisms and applications: Journal of Structural Geology, **86**, 95–152, doi: 10.1016/j.jsg.2015.09.006.

Wang, Z., S. Huang, D. Gong, W. Wu, and C. Yu, 2013, Geochemical characteristics of natural gases in the Upper Triassic Xujiahe Formation in the southern Sichuan Basin, SW China: International Journal of Coal Geology, **120**, 15–23, doi: 10.1016/j.coal.2013.09.002.

Wibberley, C. A. J., and T. Shimamoto, 2005, Earthquake slip weakening and asperities explained by thermal

pressurization: Nature, **436**, 689–692, doi: 10.1038/nature03901.

Wilson, J. E., J. E. Chester, and F. M. Chester, 2003, Microfracture analysis of fault growth and wear processes, Punchbowl Fault, San Andreas system, California: Journal of Structural Geology, **25**, 1855–1873, doi: 10.1016/S0191-8141(03)00036-1.

Xu, S., Y. Ben-Zion, and J. P. Ampuero, 2012, Properties of inelastic yielding zones generated by in-plane dynamic ruptures — 2: Detailed parameter-space study: Geophysical Journal International, **191**, 1343–1360, doi: 10.1111/j.1365-246X.2012.05685.x.

Yue, D., S. Wu, Z. Xu, X. Liang, D. Chen, Y. Ji, and Y. Zhou, 2018, Reservoir quality, natural fractures, and gas productivity of upper Triassic Xujiahe tight gas sandstones in western Sichuan Basin, China: Marine and Petroleum Geology, **89**, 370–386, doi: 10.1016/j.marpetgeo.2017.10.007.

Zou, C. N., R. K. Zhu, K. Y. Liu, L. Su, B. Bai, X. X. Zhang, X. J. Yuan, and J. H. Wang, 2012, Tight gas sands reservoirs in China: Characteristics and recognition criteria: Journal of Petroleum Science and Engineering, **88**, 82–91, doi: 10.1016/j.petrol.2012.02.001.

Biographies and photographs of authors are not available.